Pergamon

*Int. J. Heat Mass Transfer.* Vol. 39, No. 11, pp. 2195–2204, 1996

0017-9310/96 $15.00 + 0.00

0017-9310(95)00335-5

# Experimental study of the fundamental properties of reciprocating chillers and their relation to thermodynamic modeling and chiller design

H. T. CHUA, K. C. NG and J. M. GORDON†

Department of Mechanical and Production Engineering, National University of Singapore, 10 Kent Ridge Crescent, Singapore 0511

(*Received* 14 *November* 1994 *and in final form* 29 *August* 1995)

**Abstract**—From detailed experimental measurements on commercial reciprocating chillers, the loss mechanisms that dominate chiller performance can be identified, quantified and incorporated into a general irreversible thermodynamic model for predicting chiller behavior. The data can also be used to demonstrate the weaknesses and inaccuracies of a host of endoreversible chiller models that have been presented, where the primary sources of internal dissipation have been ignored. We quantitatively establish the dominant contributions to chiller performance of internal irreversibilities, such as fluid friction in the compressor and evaporator, and of finite-rate heat transfer at the heat exchangers. Heat leaks are measured experimentally and shown to be close to negligible. The empirical wisdom that has evolved in the commercial production of reciprocating chillers, namely, that rated capacity operation corresponds to near maximum efficiency, is explained in terms of a general thermodynamic model. Taking account of constraints of heat exchanger size and cost, we use experimental data to show that simple thermodynamic modeling can account for the optimal designs that are produced by the chiller industry. Copyright © 1996 Elsevier Science Ltd.

## 1. INTRODUCTION

In this paper, two issues are addressed that are fundamental to understanding the operation and thermodynamic performance of chillers:

(1) identification and quantitative evaluation of the primary irreversibility mechanisms, such that key performance variables can be evaluated accurately from first principles and

(2) revealing the empirical wisdom that has evolved in the design of commercial chillers, in terms of their nominal rated operating points corresponding to maximum-efficiency operation.

By the rubric chillers, we refer to general cooling devices, often alternatively referred to as refrigeration units and heat pumps. Our attention is restricted to reciprocating chillers (see Fig. 1 for a schematic diagram), which represent the overwhelming majority of chiller installations and cooling energy consumption in the world. We aspire to cast the problem in as general a thermodynamic framework as possible, in the spirit of recently-published universal thermodynamic models for a range of chiller types, including reciprocating chillers [1–3].

The first objective is of practical interest for a num-

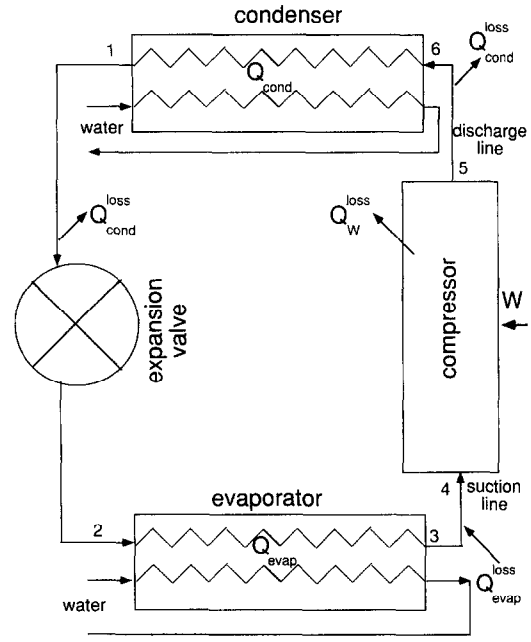


Fig. 1. Schematic diagram of water-cooled reciprocating chiller (heat pump), in which the directions of flow of refrigerant, coolant and energy are indicated.

†On sabbatical leave from: Center for Energy and Environmental Physics, Jacob Blaustein Institute for Desert Research, Ben-Gurion University of the Negev, Sede Boqer Campus 84990, Israel, and The Pearlstone Center for Aeronautical Engineering Studies, Department of Mechanical Engineering, Ben-Gurion University of the Negev, Beersheva 84105, Israel. Author to whom correspondence should be addressed.

## NOMENCLATURE

| | |
|---|---|
| $C$ | coolant specific heat |
| COP | coefficient of performance (chiller cooling capacity divided by compressor input power) |
| $E$ | heat exchanger effectiveness |
| $K$ | constant total thermal inventory defined in equation (9) |
| $m$ | coolant mass flow rate |
| $Q_{cond}$ | rate of heat rejection at the condenser |
| $Q_{cond}^{loss}$ | rate of heat leak from hot refrigerant to ambient at the condenser |
| $Q_{evap}$ | rate of heat absorbed at the evaporator = cooling capacity |
| $Q_{evap}^{loss}$ | rate of heat leak from ambient to the cold refrigerant at the evaporator |
| $Q_s^{loss}$ | defined as $Q_{evap}^{loss} - Q_{cond}^{loss} - Q_W^{loss}$ for conciseness of notation in equations (5)–(7) |
| $Q_W^{loss}$ | rate of heat leak from the compressor shell to ambient |
| $\Delta S_{int}$ | chiller internal entropy generation, due primarily to fluid friction losses in non-isentropic compression and expansion |
| $T_{cond}$ | refrigerant temperature at the condenser |
| $T_{cond}^{in}$ | condenser coolant inlet temperature |
| $T_{evap}$ | refrigerant temperature at the evaporator |
| $T_{evap}^{in}$ | evaporator coolant inlet temperature |
| $W$ | electrical power input to the compressor. |

ber of reasons. First, identification of the principal loss mechanisms enables the designer to pinpoint areas for improvement and to find problems quickly when performance degradation occurs. The two major irreversibilities are fluid friction (in the compressor and expansion device), and heat transfer (at the heat exchangers). The former disfavors low cooling rates, while the latter militates against high cooling rates. A point of maximum chiller Coefficient Of Performance (COP) is implied (see Fig. 2) and, in practical chiller design, should fall near the maximum cooling capacity, which is dictated by mechanical and material constraints. (COP is defined as cooling capacity divided by input power.) Furthermore, the kind of detailed measurements and energy bookkeeping presented here has not, to the best of the authors' knowledge, been offered within the framework of general thermodynamic modeling.

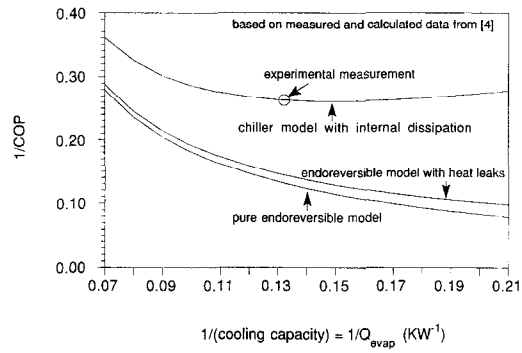


Fig. 2. Characteristic chiller curve, a plot of 1/COP against 1/(cooling capacity), at fixed coolant temperatures, for the water-cooled reciprocating chiller reported in [4]. Chiller variables are listed in Table 1. The upper-most curve is calculated with equation (5), based on experimental measurements. The single point shown corresponds to test conditions with the same water temperatures at condenser inlet and evaporator inlet. Chillers are usually designed to have maximum cooling capacity close to this point. The two lower curves are calculated from the pure endoreversible chiller model (finite-rate heat transfer being the sole irreversibility), and from an endoreversible chiller model with heat leaks, where the heat exchanger and heat leak thermal conductance have been measured experimentally (i.e. no adjustable parameters).

Second, manufacturer catalog data are usually not extensive enough to permit evaluations of the type offered here. With the experimental measurements reported here, we can confirm the contributions of each principal irreversibility source to chiller performance, and ascertain the validity of basic thermodynamic modeling procedures.

Third, the general theoretical models that have emerged from a finite-time thermodynamics approach have, for the most part, omitted the modeling of the largest irreversibilities. Consequently, their predictions stand in dramatic contrast to actual experimental performance data for chillers. Quite a few studies published to date [5–16] propose the endoreversible chiller as a model for real chillers; a system in which the only irreversibility mechanism is finite-rate heat transfer. As will be demonstrated quantitatively in Section 3, the predictions of the endoreversible chiller model are not only qualitatively incorrect, in that they indicate that chiller COP should uniformly decrease as cooling capacity increases, but they are quantitatively deficient in that predicted chiller COPs are much larger than actual experimental values.

Fourth, there is value in using theoretical models to correlate performance data, as shown in [1, 17], because such correlations can be used to estimate the cooling requirements of proposed installations.

Endoreversible chiller models supplemented with heat leaks have also been proposed [7, 17–19], their virtue being a prediction of a point of maximum COP, as opposed to the pure endoreversible model where

COP increases monotonically to its maximum Carnot value in the limit of vanishing cooling capacity. In [7, 17], this type of chiller model was intended for *cryogenic* refrigerators, where heat leaks are often considerable. However, as we will establish in Section 3, these modified models still fail to capture the principal loss mechanisms associated with internal entropy generation in *commercial reciprocating* chillers, and hence offer predictions that are distant from reality. By inserting experimentally-measured heat leak and heat exchanger values, we show that the predictions of these models are far different than actual chiller performance. The reason is simply their having ignored the irreversibilities that dominate chiller performance: fluid friction in the compressor, throttling in the evaporator and de-superheating in the condenser, in short, internal sources of entropy generation.

The second objective will help to place the empirical realities of commercial chiller development within the framework of general irreversible thermodynamic models. Maximum cooling capacity is usually dictated by mechanical and material constraints. However chiller COP and its dependence on cooling rate derive from properties of individual chiller components that represent a broad range of design options. Best results are obtained when maximum cooling capacity corresponds approximately to maximum COP. We will show that this is the situation to which chiller design has empirically evolved.

## 2. BASIC THERMODYNAMIC ELEMENTS OF CHILLER PERFORMANCE

A general thermodynamic model will now be derived, which will guide the selection of experimental measurements and their interpretation. We adopt the same general approach as in the universal thermodynamic chiller models developed in [1–3]. We focus attention on the steady-state cyclic operation of the chiller (schematic in Fig. 1); transients are neglected. All energy flows cited below are defined as positive, and refer to *cycle-averaged* values (and are hence in watts). From the first law of thermodynamics and the fact that the change in the internal energy of the chiller refrigerant is zero for a cyclic process (internal energy being a state function), one obtains:

$$Q_{\text{cond}} + Q_{\text{cond}}^{\text{loss}} - (Q_{\text{evap}} + Q_{\text{evap}}^{\text{loss}}) - (W - Q_{\text{W}}^{\text{loss}}) = 0 \tag{1}$$

where

$Q_{\text{cond}}$ = rate of heat rejection at the condenser;
$Q_{\text{cond}}^{\text{loss}}$ = rate of heat leak from the refrigerant to ambient at the condenser;
$Q_{\text{evap}}$ = rate of heat absorbed at the evaporator = cooling capacity;
$Q_{\text{evap}}^{\text{loss}}$ = rate of heat leak from ambient to the refrigerant at the evaporator;
$W$ = electrical power input to the compressor and
$Q_{\text{W}}^{\text{loss}}$ = rate of heat leak from the compressor shell to ambient.

Since entropy is also a state function, its net change over the cycle is also zero. We divide contributions to the entropy into those stemming from heat transfer (at the condenser and evaporator) and those due to internal dissipation, so that one obtains:

$$\frac{Q_{\text{cond}} + Q_{\text{cond}}^{\text{loss}}}{T_{\text{cond}}} - \frac{Q_{\text{evap}} + Q_{\text{evap}}^{\text{loss}}}{T_{\text{evap}}} - \Delta S_{\text{int}} = 0 \tag{2}$$

where $T_{\text{cond}}$ and $T_{\text{evap}}$ are the refrigerant temperatures at the condenser and evaporator, respectively, and $\Delta S_{\text{int}}$ represents internal dissipation due to non-isentropic compression and expansion over the cycle. In equation (2), heat transfer need not be viewed as occurring isothermally; rather the refrigerant temperatures represent their process-average values, specifically, the ratio of enthalpy change to entropy change during heat exchange [20]. We have also viewed the dissipation due to pressure drop in the condenser and evaporator as negligible, so that heat transfer at each stage can be equated to the change in the enthalpy of the refrigerant.

Next, we relate refrigerant temperatures to fluid coolant temperatures, for which we invoke the energy balance relations at the heat exchangers [21]:

$$Q_{\text{cond}} = (mCE)_{\text{cond}}(T_{\text{cond}} - T_{\text{cond}}^{\text{in}}) \tag{3}$$

$$Q_{\text{evap}} = (mCE)_{\text{evap}}(T_{\text{evap}}^{\text{in}} - T_{\text{evap}}) \tag{4}$$

where $m$ = mass flow rate; $C$ = coolant specific heat; $E$ = heat exchanger effectiveness; $T_{\text{cond}}^{\text{in}}$ = condenser coolant inlet temperature and $T_{\text{evap}}^{\text{in}}$ = evaporator coolant inlet temperature. Combining equations (1)–(4) and eliminating the refrigerant temperatures in favor of the more readily measured coolant temperatures, one obtains an analytic formula for COP as a function of cooling capacity, coolant temperatures, heat exchanger characteristics, heat leak terms, and internal losses $\Delta S_{\text{int}}$. The characteristic chiller curve is conveniently expressed as 1/COP as a function of $1/Q_{\text{evap}}$:

$$1/\text{COP} = \left\{ -1 + \frac{T_{\text{cond}}^{\text{in}} \Delta S_{\text{int}} + Q_{\text{W}}^{\text{loss}} - Q_{\text{evap}}^{\text{loss}}}{Q_{\text{evap}}} \right.$$
$$+ \left[1 + \frac{Q_{\text{evap}}^{\text{loss}}}{Q_{\text{evap}}}\right] \left[ \frac{\dfrac{T_{\text{cond}}^{\text{in}}}{Q_{\text{evap}}}}{\dfrac{T_{\text{evap}}^{\text{in}}}{Q_{\text{evap}}} - \dfrac{1}{(mCE)_{\text{evap}}}} \right]$$
$$\left. + \frac{1 + \dfrac{Q_{\text{evap}}^{\text{loss}} + Q_{\text{s}}^{\text{loss}}}{Q_{\text{evap}}} + \dfrac{Q_{\text{s}}^{\text{loss}} Q_{\text{evap}}^{\text{loss}}}{Q_{\text{evap}}^2}}{(mCE)_{\text{cond}} \left[ \dfrac{T_{\text{cond}}^{\text{in}}}{Q_{\text{evap}}} - \dfrac{1}{(mCE)_{\text{evap}}} \right]} \right\}$$

$$+\frac{\Delta S_{\text{int}}}{(mCE)_{\text{cond}}}\left[1+\frac{Q_{\text{s}}^{\text{loss}}}{Q_{\text{evap}}}\right]\Bigg\}$$

$$\cdot\left[1-\frac{\Delta S_{\text{int}}}{(mCE)_{\text{cond}}}-\frac{\left[1+\dfrac{Q_{\text{evap}}^{\text{loss}}}{Q_{\text{evap}}}\right]}{(mCE)_{\text{cond}}\left[\dfrac{T_{\text{evap}}^{\text{in}}}{Q_{\text{evap}}}-\dfrac{1}{(mCE)_{\text{evap}}}\right]}\right]^{-1} \tag{5}$$

where for conciseness of notation, we have defined

$$Q_{\text{s}}^{\text{loss}}=Q_{\text{evap}}^{\text{loss}}-Q_{\text{cond}}^{\text{loss}}-Q_{\text{W}}^{\text{loss}}. \tag{6}$$

Figures 2 and 3 include sample plots of equation (5), and show the basic performance features: (a) a (linear) regime at relatively low cooling capacity, where chiller behavior is dominated by internal losses; (b) a region at relatively high cooling capacity where heat transfer is the key bottleneck and COP changes rapidly with cooling rate and (c) a point of maximum COP at the optimal balance between internal dissipation and heat transfer losses.

For many chiller types, such as centrifugal, thermoelectric and others, much of the characteristic chiller curve shown in Fig. 2 can be accessed experimentally [3]. For reciprocating chillers, however, once one fixes the coolant temperatures, only a single point can be measured for a given (theoretical) curve. For different coolant temperatures, each performance point corresponds to a different curve, as illustrated in Figs. 2–4. The theoretical curves correspond to varying cooling capacity by changing *refrigerant* temperatures (at fixed *coolant* temperatures). They are a hypothetical construct that illustrates the nature of chiller operation and shows where actual operating points lie relative to maximum-COP operation.

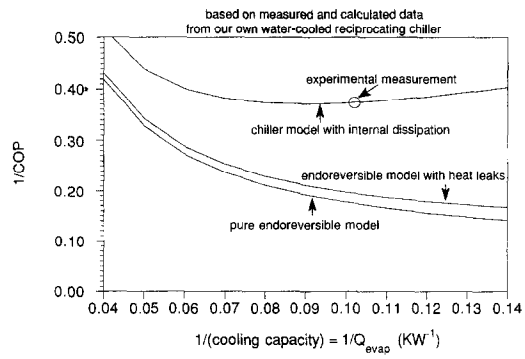


Fig. 3. Characteristic chiller performance curve, for our own water-cooled reciprocating chiller. Chiller variables are listed in Table 2. The upper-most curve is calculated with equation (5), based on experimental measurements. The single point shown corresponds to standard rated operating conditions [26].

In the limiting case of no internal losses ($\Delta S_{\text{int}}=0$), one obtains the results for the endoreversible chiller with heat leaks:

$$1/\text{COP}=\Bigg\{-1+\frac{Q_{\text{W}}^{\text{loss}}-Q_{\text{evap}}^{\text{loss}}}{Q_{\text{evap}}}$$

$$+\left[1+\frac{Q_{\text{evap}}^{\text{loss}}}{Q_{\text{evap}}}\right]\left[\frac{\dfrac{T_{\text{cond}}^{\text{in}}}{Q_{\text{evap}}}}{\dfrac{T_{\text{evap}}^{\text{in}}}{Q_{\text{evap}}}-\dfrac{1}{(mCE)_{\text{evap}}}}\right]$$

$$+\frac{1+\dfrac{Q_{\text{evap}}^{\text{loss}}+Q_{\text{s}}^{\text{loss}}}{Q_{\text{evap}}}+\dfrac{Q_{\text{s}}^{\text{loss}}Q_{\text{evap}}^{\text{loss}}}{Q_{\text{evap}}^{2}}}{(mCE)_{\text{cond}}\left[\dfrac{T_{\text{cond}}^{\text{in}}}{Q_{\text{evap}}}-\dfrac{1}{(mCE)_{\text{evap}}}\right]}\Bigg\}$$

$$\cdot\left[1-\frac{\left[1+\dfrac{Q_{\text{evap}}^{\text{loss}}}{Q_{\text{evap}}}\right]}{(mCE)_{\text{cond}}\left[\dfrac{T_{\text{evap}}^{\text{in}}}{Q_{\text{evap}}}-\dfrac{1}{(mCE)_{\text{evap}}}\right]}\right]^{-1} \tag{7}$$

and when the heat leaks are ignored, the simple endoreversible formula emerges:

$$1/\text{COP}=\Bigg\{-1+\frac{\dfrac{T_{\text{cond}}^{\text{in}}}{Q_{\text{evap}}}}{\dfrac{T_{\text{evap}}^{\text{in}}}{Q_{\text{evap}}}-\dfrac{1}{(mCE)_{\text{evap}}}}$$

$$+\frac{1}{(mCE)_{\text{cond}}\left[\dfrac{T_{\text{cond}}^{\text{in}}}{Q_{\text{evap}}}-\dfrac{1}{(mCE)_{\text{evap}}}\right]}\Bigg\}$$

$$\cdot\left[1-\frac{1}{(mCE)_{\text{cond}}\left[\dfrac{T_{\text{evap}}^{\text{in}}}{Q_{\text{evap}}}-\dfrac{1}{(mCE)_{\text{evap}}}\right]}\right]^{-1}. \tag{8}$$

These curves are also shown in Figs. 2 and 3.

## 3. EXPERIMENTAL MEASUREMENTS FOR WATER-COOLED CHILLERS

### 3.1. *Measured data*

Two water-cooled reciprocating chillers, typical of currently-available commercial chillers, are taken as representative examples. One source of data is taken from the experimental study of Liang and Kuehn [4], the data of which are summarized in Table 1. These

Table 1. Measured and calculated data for the water-to-water heat pump, as reported in [4]

| Chiller variable | Measured value |
|---|---|
| Refrigerant | Freon R-22 |
| Refrigerant mass flow rate | 0.0414 kg $s^{-1}$ |
| Electrical power input to compressor | 1.99 kW |
| Heat leak from compressor to ambient | 0.08 kW |
| Condenser water inlet temperature | 9.33°C |
| Evaporator water inlet temperature | 9.28°C |
| Cooling capacity | 7.56 kW |
| 1/COP | 0.263 |

Refrigerant thermodynamic properties at the six states indicated in Fig. 1 (from [4])

| | Measured | | Calculated | | |
|---|---|---|---|---|---|
| State | Pressure [MPa] | Temperature [K] | Specific enthalpy [kJ $kg^{-1}$] | Specific entropy [kJ $kg^{-1}$ $K^{-1}$] | Specific volume [$m^3$ $kg^{-1}$] |
| 1 | 0.9268 | 293.8 | 103.19 | 0.4172 | 0.00083 |
| 2 | 0.4367 | 269.2 | 103.19 | 0.4234 | 0.00823 |
| 3 | 0.4254 | 273.8 | 285.64 | 1.1032 | 0.05635 |
| 4 | 0.3964 | 277.8 | 289.03 | 1.1218 | 0.06209 |
| 5 | 1.0480 | 352.3 | 335.19 | 1.1831 | 0.02937 |
| 6 | 1.0411 | 347.7 | 331.66 | 1.1736 | 0.02905 |

data translate into a single point on the chiller performance curve in Fig. 2.

The other data are measurements in our experimental chiller facility at the National University of Singapore. Details of the chiller and of our experimental procedures have been reported in [22–25]. As a brief summary, we note that heat leaks from exposed piping were determined from measurements of refrigerant mass flow rate and changes in specific enthalpy (enthalpy being computed from pressure and temperature measurements). Heat leaks at the insulated heat exchangers were computed from the difference in the enthalpy changes of the refrigerant and the coolant. Since the heat leaks at the condenser and evaporator are relatively small, and since they are obtained from differences in absolute enthalpy, the uncertainty in their measurement is high, relative to their absolute values, as is evident from the figures listed in Table 2.

Our own data are listed in Table 2, including experimental uncertainties. The measured point at standard rated operating conditions [26] is shown in Fig. 3 along with the corresponding performance curve. Several of our measured points, each on its own characteristic chiller curve, are shown in Figs. 3 and 4. Both our chiller and the chiller reported in [4] are relatively small (between 7 and 13 KW cooling capacity), with significantly different COPs that stem mainly from large differences in the relative contribution of internal dissipation.

Note that all coolant temperatures, heat exchanger properties, flow rates, and heat leaks have been measured directly. Internal entropy generation $\Delta S_{int}$ was computed from the entropy difference between the condenser and the evaporator by using simultaneous measurements of the refrigerant's pressure, temperature and flow rates.

### 3.2. *Implications for chiller operating range and thermodynamic models*

We have calculated the chiller performance curves with equation (5) and plotted them in Figs. 2–4. The fact that data points lie exactly on the predicted curves is not a test of theoretical predictions. Rather it is simply a confirmation of the accuracy of the experimental measurements and the fact that all energy flows have been accounted for in equation (1). It is the entropy-balance equation (2) [and the final result of equation (5) that derives from it] that determines *where* along the chiller performance curve the operating points lie.

In light of the plethora of endoreversible thermodynamic models proposed for chillers, including those which include heat leaks, we used the experimental measurements to generate the chiller curves that correspond to a pure endoreversible chiller, and to the endoreversible chiller with heat leaks. These curves are shown for each of the two reciprocating chillers in Figs. 2 and 3. Note that these calculated curves involve no adjustable parameters. The comparison between the data-based chiller curves and the curves based on the endoreversible models clearly indicates the dominant contribution of internal losses to chiller COP, at least for realistic chiller operating conditions. Finite-rate heat transfer by itself (the pure endoreversible model) is an important element, but inadequate as a complete model for *real* chillers. The introduction of heat leaks in principle gives rise to a

Table 2. Summary of all experimental measurements for the water-cooled chiller reported here, including experimental uncertainties. Refrigerant is Freon R-22

| | $T_{cond}^{in}$ [°C] ±0.05 | $T_{evap}^{in}$ [°C] ±0.05 | $Q_{cond}$ [kW] ±0.2 | $Q_{evap}$ [kW] ±0.2 | $W$ [kW] ±0.01 | 1/COP ±0.006 | $Q_{cond}^{loss}$ [kW] ±0.4 | $Q_{evap}^{loss}$ [kW] ±0.3 | $\Delta S_{int}$ [kW K$^{-1}$] ±0.0003 | $Q_{W}^{loss}$ [kW] ±0.01 | $(mCE)_{cond}$ [kW K$^{-1}$] ±0.04 | $(mCE)_{evap}$ [kW K$^{-1}$] ±0.05 |
|---|---|---|---|---|---|---|---|---|---|---|---|---|
| b | 24.09 | 8.02 | 13.8 | 9.8 | 3.66 | 0.373 | −0.173 | 0.289 | 0.00531 | 0.127 | 0.840 | 0.608 |
| | 23.89 | 10.00 | 14.5 | 10.5 | 3.71 | 0.353 | 0.017 | 0.358 | 0.00537 | 0.082 | 0.884 | 0.622 |
| | 23.81 | 12.37 | 15.3 | 11.4 | 3.81 | 0.336 | 0.043 | 0.318 | 0.00539 | 0.110 | 0.918 | 0.643 |
| c | 23.94 | 13.96 | 15.6 | 11.7 | 3.84 | 0.329 | 0.075 | 0.306 | 0.00528 | 0.133 | 0.905 | 0.639 |
| | 23.90 | 15.99 | 16.3 | 12.4 | 3.90 | 0.315 | 0.053 | 0.191 | 0.00529 | 0.118 | 0.907 | 0.646 |
| d | 23.88 | 18.00 | 16.8 | 12.9 | 3.92 | 0.302 | 0.044 | 0.114 | 0.00520 | 0.135 | 0.917 | 0.649 |
| | 26.75 | 8.00 | 13.7 | 9.8 | 3.74 | 0.380 | −0.035 | 0.227 | 0.00526 | 0.152 | 0.869 | 0.618 |
| | 26.75 | 10.00 | 14.4 | 10.5 | 3.81 | 0.364 | −0.010 | 0.238 | 0.00539 | 0.122 | 0.900 | 0.640 |
| | 26.75 | 12.41 | 15.3 | 11.3 | 3.94 | 0.348 | 0.006 | 0.230 | 0.00555 | 0.130 | 0.939 | 0.672 |
| | 26.67 | 14.00 | 15.9 | 11.9 | 3.98 | 0.335 | −0.003 | 0.187 | 0.00557 | 0.117 | 0.953 | 0.689 |
| | 26.74 | 16.01 | 16.8 | 12.7 | 4.10 | 0.322 | 0.057 | 0.156 | 0.00578 | 0.100 | 0.992 | 0.716 |
| | 26.67 | 17.99 | 17.6 | 13.4 | 4.14 | 0.308 | 0.105 | 0.196 | 0.00576 | 0.076 | 1.007 | 0.734 |
| | 29.49 | 8.00 | 13.3 | 9.4 | 3.85 | 0.408 | 0.059 | 0.261 | 0.00537 | 0.170 | 0.817 | 0.602 |
| | 29.38 | 10.00 | 14.1 | 10.1 | 3.91 | 0.388 | −0.005 | 0.213 | 0.00536 | 0.140 | 0.853 | 0.595 |
| a | 29.43 | 12.39 | 14.7 | 10.7 | 3.98 | 0.373 | 0.006 | 0.219 | 0.00511 | 0.195 | 0.838 | 0.594 |
| | 29.43 | 13.98 | 15.6 | 11.4 | 4.09 | 0.357 | 0.081 | 0.189 | 0.00567 | 0.087 | 0.884 | 0.659 |
| | 29.39 | 15.97 | 16.3 | 12.1 | 4.17 | 0.345 | 0.075 | 0.187 | 0.00566 | 0.099 | 0.907 | 0.665 |
| | 29.41 | 17.99 | 17.1 | 12.9 | 4.22 | 0.328 | 0.143 | 0.147 | 0.00573 | 0.034 | 0.949 | 0.668 |
| | 32.19 | 7.98 | 13.2 | 9.2 | 3.94 | 0.428 | 0.014 | 0.223 | 0.00543 | 0.159 | 0.794 | 0.581 |
| | 32.24 | 10.00 | 14.1 | 9.9 | 4.04 | 0.406 | −0.013 | 0.212 | 0.00556 | 0.147 | 0.831 | 0.631 |
| | 32.22 | 12.40 | 15.0 | 10.8 | 4.16 | 0.386 | −0.108 | 0.162 | 0.00551 | 0.191 | 0.885 | 0.644 |
| | 32.18 | 13.99 | 15.6 | 11.3 | 4.25 | 0.375 | −0.025 | 0.162 | 0.00566 | 0.183 | 0.895 | 0.673 |
| | 32.22 | 16.01 | 16.4 | 12.1 | 4.32 | 0.357 | 0.000 | 0.140 | 0.00578 | 0.122 | 0.922 | 0.695 |
| | 32.26 | 18.02 | 17.2 | 12.8 | 4.43 | 0.347 | 0.026 | 0.190 | 0.00579 | 0.131 | 0.928 | 0.711 |
| e | 34.99 | 8.01 | 13.0 | 8.9 | 4.01 | 0.450 | −0.174 | 0.148 | 0.00527 | 0.215 | 0.722 | 0.577 |
| | 34.88 | 10.00 | 13.7 | 9.5 | 4.10 | 0.429 | −0.048 | 0.178 | 0.00540 | 0.175 | 0.750 | 0.603 |
| | 35.01 | 12.40 | 14.8 | 10.4 | 4.26 | 0.408 | −0.075 | 0.172 | 0.00565 | 0.145 | 0.818 | 0.633 |
| f | 34.97 | 13.99 | 15.4 | 11.0 | 4.36 | 0.396 | −0.042 | 0.172 | 0.00575 | 0.152 | 0.852 | 0.648 |
| | 35.05 | 15.98 | 16.2 | 11.7 | 4.45 | 0.379 | −0.093 | 0.088 | 0.00581 | 0.150 | 0.895 | 0.667 |
| g | 34.99 | 17.99 | 16.9 | 12.5 | 4.55 | 0.366 | 0.045 | 0.099 | 0.00590 | 0.154 | 0.901 | 0.702 |

a : standard rating conditions for chiller tests ; b : measured point in Figs. 2–5 ; c,d,e,f,g : measured points in Fig. 4.

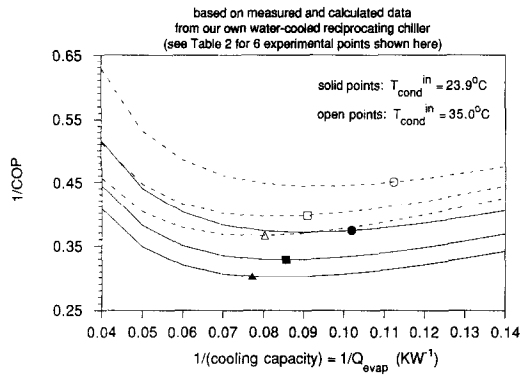


Fig. 4. Characteristic chiller plots for six sets of coolant temperatures, for our own water-cooled chiller. Chiller variables are listed in Table 2. Each measured point lies on a separate curve which is calculated with equation (5) and based on experimental measurements. Note that in each instance chiller performance is close to its maximum-COP point.

maximum COP point. However, for actual heat leak values, the predicted maximum COP point is so far from the actual one, and at such high values of COP, as to render these chiller models untenable.

The curves in Figs. 2–4 provide a quantitative view of the contribution of the key loss mechanisms to chiller performance, and how they vary with operating conditions. Heat transfer and fluid friction are the dominant factors, the former growing increasingly important at high cooling rates and the latter being significant at low cooling rates. Heat leaks play a negligible role. Furthermore, it is easy to evaluate how a given alteration of heat exchanger, compressor or throttling characteristics will modify chiller COP as well as the part of the performance curve on which the chiller operates.

These curves are also revealing in that they point to the empirical wisdom embedded in the evolution of commercial reciprocating chillers. Specifically, these chillers have been developed so that their nominal maximum-capacity operating point is around the maximum COP point (the minimum in the curves in Figs 2–4). The extremum is a broad one. Around the maximum-COP point, chiller performance is more tolerant to changes in cooling capacity on the low-cooling-rate side. Hence one would expect chiller design to accommodate a range of operating conditions *below* maximum capacity that fall to the right of the maximum COP point in Figs. 2–4. This is exactly what is observed.

## 4. CONSTRAINED CHILLER OPTIMIZATION FOR LIMITED HEAT EXCHANGER SIZE

### 4.1. *Water-cooled chillers*

The chiller's thermal inventory [$(mCE)_{cond}$ and $(mCE)_{evap}$ in equations (3) and (4)] is an expensive commodity. Higher ($mCE$) values ensure higher COPs, but increase heat exchanger size and pumping costs. As noted above, commercial reciprocating chillers appear to be built for an operating range where internal losses are balanced against the thermal inventory bottleneck. Therefore chiller COP will not be insensitive to changes in heat exchanger size or coolant flow rates.

To illustrate how the thermodynamic model cited above can be used to determine the component parameters for maximum-COP performance when practical cost constraints are introduced, we consider the chiller's total thermal inventory as a design constraint [27], namely

$$(mCE)_{cond} + (mCE)_{evap} = \text{constant} \equiv K. \quad (9)$$

Earlier studies of the impact of the constraint of fixed total heat exchanger thermal conductance or fixed total heat exchanger size include [5, 17, 28], although no comparisons with actual chiller constructions were attempted.

The predictions of equation (5), subject to equation (9) are plotted in Fig. 5, a three-dimensional plot of 1/COP as a function of 1/(cooling capacity) and evaporator thermal inventory. The standard rating point of our water-cooled chiller is also shown, and attests to chiller design being rather close to the calculated optimum.

In this study, all the variables in equation (5) and (9) have been measured. Hence we can compare actual chiller designs against the results of the constrained optimization calculation. The relevant figures are summarized in Table 3 for the two water-cooled chillers analyzed. The maximum-COP operating conditions have been calculated from our model by applying to equations (5)

$$\partial(\text{COP})/\partial(Q_{evap}) = 0 \quad (10)$$

and

$$\partial(\text{COP})/\partial(mCE)_{evap} = 0 \quad (11)$$

subject to the limiting inequality

$$Q_{evap} < (mCE)_{evap} T_{evap}^{in} \{K - (mCE)_{evap} - \Delta S_{int}\}/\{K - \Delta S_{int}\}. \quad (12)$$

The results cited in Table 3 appear to confirm that commercial chiller design has evolved toward the conditions that emerge from our constrained thermodynamic optimization calculation.

### 4.2. *Severely-constrained optimal designs: air-cooled chillers*

For water-cooled chillers, both the evaporator and condenser heat exchangers are situated in the same location, with little if any space constraints (beyond the cost of the heat exchanger). A practical and more severely-constrained device is the commercial air-to-air "split" chiller unit [29]. The condenser and compressor are placed outdoors. The evaporator (direct expansion cooling coil) is housed in the indoor unit,

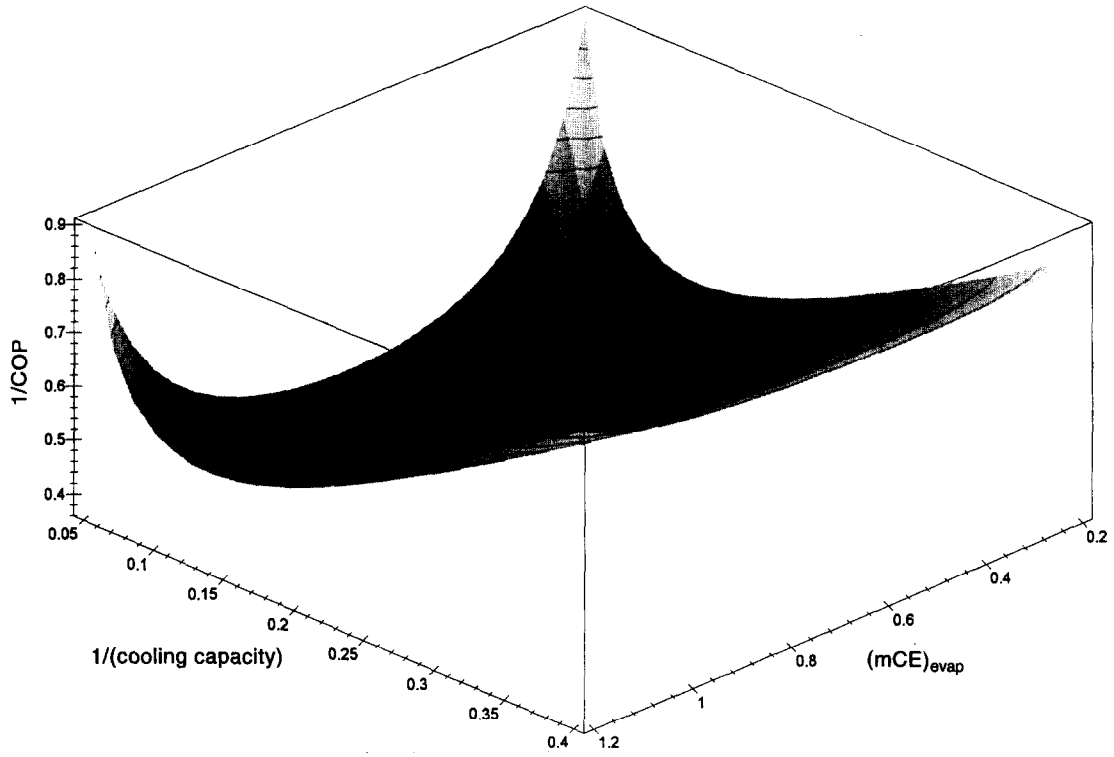


Fig. 5. Three-dimensional graph that illustrates identification of the constrained maximum-COP design conditions when the limitation of fixed total heat exchanger thermal inventory is imposed. 1/COP is plotted against 1/(cooling capacity) and against the evaporator's thermal inventory, for our water-cooled reciprocating chiller, the experimentally-measured variables of which are listed in Table 2. The darkened point indicates the standard rated operating point, which is close to the calculated optimum.

where space is often at a premium. When the indoor occupancy space is a major constraint, the chiller design would impose the *evaporator's* thermal inventory (rather than the *total* thermal inventory) as a constraint. Namely, the size of the fan coil would be selected, and the design cooling capacity would then be modified to a nominally sub-optimal value in order to accommodate the new size limitation. The question then is determination of optimal operating conditions for this differently-constrained situation.

Chiller experimental data, and the results of our constrained optimization calculations, appear in

Table 3. Experimentally-measured chiller properties and calculated optimal operating conditions for the two water-cooled chillers analyzed here at standard chiller rating conditions

| Chiller available | Our chiller | Liang and Kuehn's chiller [4] |
|---|---|---|
| $T^{in}_{cond}$ [°C] | 29.43 | 9.33 |
| $T^{in}_{evap}$ [°C] | 12.39 | 9.28 |
| $Q^{loss}_{evap}$ [kW] | 0.219 | 0.14 |
| $Q^{loss}_{cond}$ [kW] | 0.006 | 0.15 |
| $Q^{loss}_{W}$ [kW] | 0.195 | 0.08 |
| $\Delta S_{int}$ [kW K$^{-1}$] | 0.00511 | 0.00279 |
| $(mCE)_{cond}$ [kW K$^{-1}$] | 0.838 | 0.463 |
| $(mCe)_{evap}$ [kW K$^{-1}$] | 0.594 | 0.463 |
| $Q_{evap}$ (kW) | 10.66 | 7.56 |
| 1/COP | 0.373 | 0.263 |
| Calculated optimal operating conditions (from thermodynamic model) | | |
| $(mCE)^{optimal}_{evap}$ [kW K$^{-1}$] | 0.673 | 0.439 |
| $Q^{optimal}_{evap}$ [kW] | 11.45 | 6.71 |
| $(1/COP)^{optimal}$ | 0.369 | 0.261 |

Table 4. Comparison between model predictions of optimal operating conditions and experimental performance data, for commercial air-to-air split chillers [29], at rated coolant temperatures $T_{cond}^{in} = 35.0°C$ and $T_{evap}^{in} = 27.0°C$. In particular, compare the values of measured and predicted cooling capacity ($Q_{evap}$) and COP for each chiller.

| Model no. | 38 PE008 | 38 PE009 | 38 PE010 | 38 PE012 | 38 PE015 | 38 PE018 | 38 PE020 | 38 PE025 | 38 PE030 | 38 PE036 | 38 PE045 |
|---|---|---|---|---|---|---|---|---|---|---|---|
| Computed and measured data from manufacturer [29]: | | | | | | | | | | | |
| $\Delta S_{int}$ [kW K$^{-1}$] computed | 0.012 | 0.013 | 0.016 | 0.013 | 0.015 | 0.022 | 0.029 | 0.025 | 0.028 | 0.043 | 0.066 |
| $(mCE)_{evap}$ [kW K$^{-1}$] computed | 0.781 | 1.021 | 1.101 | 1.224 | 1.672 | 2.048 | 2.180 | 2.422 | 4.772 | 4.055 | 4.898 |
| $(mCE)_{cond}$ [kW K$^{-1}$] computed | 1.739 | 2.053 | 2.389 | 2.649 | 2.925 | 3.731 | 4.623 | 4.975 | 5.167 | 7.536 | 9.956 |
| $Q_{evap}$ [kW] measured | 18.6 | 23.3 | 26.0 | 29.1 | 36.6 | 46.5 | 52.3 | 58.1 | 73.3 | 93.0 | 116.0 |
| 1/COP measured | 0.368 | 0.345 | 0.361 | 0.306 | 0.303 | 0.323 | 0.348 | 0.309 | 0.271 | 0.319 | 0.356 |
| Constraint: fixed *evaporator* heat exchanger thermal inventory. Optimal operating conditions for maximum COP: | | | | | | | | | | | |
| $Q_{evap}$ [kW] | 20.6 | 24.6 | 28.3 | 27.4 | 34.2 | 45.1 | 54.1 | 53.4 | 71.6 | 88.8 | 121.9 |
| 1/COP | 0.366 | 0.344 | 0.360 | 0.306 | 0.302 | 0.323 | 0.348 | 0.308 | 0.271 | 0.318 | 0.356 |

Table 4. In [29], sufficient experimental data were reported for 11 air-cooled reciprocating chillers to permit evaluation of all chiller variables listed in Table 4. In our calculation of COP, the chiller input power does not include the small contributions from the condenser and evaporator fans. The close agreement between predicted constrained optima and the actual design operating conditions of these chillers appears to support the assumptions about the limitations that dictate chiller design as well as our thermodynamic model.

Six characteristic performance curves for one of these chillers are plotted in Fig. 6. They again point to commercial reciprocating air-cooled chillers being tailored to approximately maximum-COP operating conditions. In air-cooled chillers, one expects heat exchangers to pose a larger bottleneck effect than in water-cooled chillers. This effect would manifest itself in chillers operating further to the left on the characteristic chiller plot, while still straddling the maximum-COP conditions. This too appears to be confirmed by the data-based results.

## 5. SUMMARY

Via detailed experimental measurements on several representative water-cooled and air-cooled reciprocating chillers, in concert with a general thermodynamic model for chiller performance, we have highlighted some basic chiller properties and design criteria. Specifically:

(1) Chiller performance is dominated by the competing effects of heat transfer and internal fluid friction losses. The former prevails at relatively high cooling rates, and the latter at relatively low cooling rates.

(2) Heat leaks in commercial chillers are close to negligible.

(3) Chiller models based on endoreversible behavior, even when heat leaks are accounted for, fail to account for the fundamental performance characteristics of real chillers, because they omit consideration of internal dissipation. Using actual chiller data, we have shown that their predictions of maximum COP, of cooling capacity at the maximum-

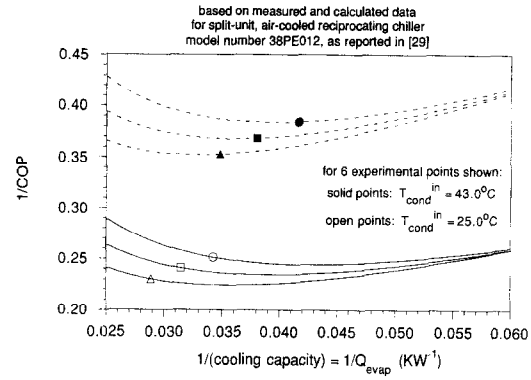


Fig. 6. Characteristic chiller plot for six sets of coolant temperatures for one of the split-unit air-cooled reciprocating chillers reported in [29]. Each measured point lies on a separate curve which is calculated based on experimental measurements. Note that chiller operation falls more to the heat-exchanger-dominated side (i.e. to the left) of the maximum-COP point than for the water-cooled chillers analyzed earlier.

COP point, and of the relation between COP and cooling capacity are markedly inaccurate.

(4) Characteristic chiller performance curves exhibit a broad maximum for COP as a function of cooling capacity and of heat exchanger thermal inventory. Deviations from maximum-efficiency behavior are more tolerant to deviations on the low-cooling-capacity side, where internal losses dominate.

(5) A simple thermodynamic model can be used to calculate optimal chiller operating conditions when the practical constraint of fixed heat exchanger thermal inventory is imposed. Predictions are in good agreement with data-based results from commercial chillers.

(6) In severely-limited chiller design, the example considered here being split air-cooled units, the simple thermodynamic model again yields predictions for optimal operating conditions that agree well with actual chiller designs.

(7) Commercial chillers appear to have evolved to designs where their rated maximum-capacity operation is close to their maximum-COP point. This reflects the empirical wisdom embedded in their design and construction.

## REFERENCES


1. J. M. Gordon and K. C. Ng, Thermodynamic modeling of reciprocating chillers, *J. Appl. Phys.* **75,** 2769–2774 (1994).
2. J. M. Gordon and K. C. Ng, A general thermodynamic model for absorption chillers: theory and experiment, *Heat Recovery Syst. Combined Heat Power* **15,** 73–83 (1995).
3. J. M. Gordon and K. C. Ng, Predictive and diagnostic aspects of a universal thermodynamic model for chillers, *Int. J. Heat Mass Transfer* **38,** 807–818 (1995).
4. H. Liang and T. H. Kuehn, Irreversibility analysis of a water-to-water mechanical-compression heat pump, *Energy Int. J.* **16,** 883–896 (1991).
5. A. Bejan, Power and refrigeration plants for minimum heat exchanger inventory, *ASME J. Energy Resour. Technol.* **115,** 148–150 (1993).
6. A. Bejan, *Entropy Generation through Heat and Fluid Flow*. Wiley, New York (1982).
7. A. Bejan, *Advanced Engineering Thermodynamics*. Wiley, New York (1988).
8. J. Chen and Z. Yan, Optimal performance of an endoreversible-combined refrigeration cycle, *J. Appl. Phys.* **63,** 4795–4798 (1988).
9. Z. Yan and J. Chen, An optimal endoreversible three-heat-source refrigerator, *J. Appl. Phys.* **65,** 1–4 (1989).
10. J. Chen and Z. Yan, Equivalent combined systems of three-heat-source heat pumps, *J. Chem. Phys.* **90,** 4951–4955 (1989).
11. J. Chen and Z. Yan, Unified description of endoreversible cycles, *Phys. Rev. A* **39,** 4140–4147 (1989).
12. D. C. Agrawal and V. J. Menon, Performance of a Carnot refrigerator at maximum cooling power, *J. Phys. A* **23,** 5319–5326 (1990).
13. Z. Yan and J. Chen, A class of irreversible Carnot refrigeration cycles with a general heat transfer law, *J. Phys. D* **23,** 136–141 (1990).
14. C. Wu, Cooling capacity optimization of a geothermal absorption refrigeration cycle, *Int. J. Ambient Energy* **13,** 133–138 (1992).
15. C. Wu, Specific heating load of an endoreversible Carnot heat pump, *Int. J. Ambient Energy* **14,** 25–28 (1993).
16. C. Wu, Performance of a solar-engine-driven-air-conditioning system, *Int. J. Ambient Energy* **14,** 77–82 (1993).
17. A. Bejan, Theory of heat transfer—irreversible refrigeration plants, *Int. J. Heat Mass Transfer* **32,** 1631–1639 (1989).
18. R. K. Pathria, J. D. Nulton and P. Salamon, Carnot-like processes in finite time—II. Applications to model cycles, *Am. J. Phys.* **61,** 916–924 (1993).
19. D. C. Agrawal and V. J. Menon, Finite-time Carnot refrigeration with wall gain and product loads, *J Appl. Phys.* **74,** 2153–2158 (1993).
20. I. Cerepnalkovski, *Modern Refrigeration Machines*. Elsevier, Amsterdam (1991).
21. W. M. Kays and A. L. London, *Compact Heat Exchangers* (2nd Edn). McGraw-Hill, New York (1964).
22. T. Y. Bong, K. C. Ng and K. O. Lau, Test facility for water-cooled water chiller, *ASHRAE Trans.* **96**(1), 205–212 (1990).
23. H. T. Chua, Performance analysis of vapour compression chillers, M.Eng. Thesis, Department of Mechanical and Production Engineering, National University of Singapore, Singapore (1995).
24. K. C. Ng, H. T. Chua, T. Y. Bong, S. S. Lee and T. K. Lee, Experimental and theoretical analysis of water-cooled chiller, *IES J. Singapore* (*Chem. Engng*) **34**(2), 45–54 (1994).
25. T. K. Lee, Performance analysis of reciprocating chillers, B.Eng. Thesis, Department of Mechanical and Production Engineering, National University of Singapore, Singapore (1994).
26. Air-Conditioning and Refrigeration Institute (ARI) Standard 590, Standard for reciprocating water-chilling packages, AIR, Arlington, VA (1986).
27. Fixed heat exchanger inventory can be represented by a number of variables that are not rigorously equivalent, e.g. total thermal conductance, total heat exchange area, cycle-average total ($mCE$), and instantaneous total ($mCE$), among others. The qualitative trends in our predictions are the same for each of these choices, although the quantitative results can vary. Which variable will be selected can be manufacturer and device-specific.
28. S. A. Klein, Design considerations for refrigeration cycles, *Int. J. Refrigeration* **15,** 181–185 (1992).
29. Toyo Carrier Engineering Co. Ltd., 38PE 40HQ, SQ, TQ split system cooling units, 50 Hz, cooling 18.6–130.2 KW, Publication ECR9105-1(S), Tokyo, Japan (1989).